Matter and Radiation at Extremes

RESEARCH ARTICLE

pubs.aip.org/aip/mre

Density-dependent carrier-envelope phase shift in attosecond pulse generation from relativistically oscillating mirrors

Cite as: Matter Radiat. Extremes 8, 064004 (2023); doi: 10.1063/5.0155957
Submitted: 25 April 2023 • Accepted: 21 August 2023 •
Published Online: 18 September 2023

Rishat Zagidullin,[1,a] Stefan Tietze,[2,3] Matt Zepf,[2,3] Jingwei Wang,[4,b] and Sergey Rykovanov[1,c]

AFFILIATIONS

[1] Center for AI Technologies, Skolkovo Institute of Science and Technology, Moscow, Russia
[2] Helmholtz-Institute Jena, Fröbelstieg 3, 07743 Jena, Germany
[3] Friedrich-Schiller-Universität Jena, Physikalisch-Astronomische Fakultät, Max-Wien-Platz 1, 07743 Jena, Germany
[4] State Key Laboratory of High Field Laser Physics and Chinese Academy of Sciences Center for Excellence in Ultra-Intense Laser Science, Shanghai Institute of Optics and Fine Mechanics, Chinese Academy of Sciences, Shanghai 201800, China

[a] **Author to whom correspondence should be addressed:** zagidullinrishat@gmail.com
[b] **Electronic mail:** wangjw@siom.ac.cn
[c] **Electronic mail:** s.rykovanov@skoltech.ru

ABSTRACT

The carrier-envelope phase (CEP) φ_0 is one of the key parameters in the generation of isolated attosecond pulses. In particular, "cosine" pulses ($\varphi_0 = 0$) are best suited for generation of single attosecond pulses in atomic media. Such "cosine" pulses have the peak of the most intense cycle aligned with the peak of the pulse envelope, and therefore have the highest contrast between the peak intensity and the neighboring cycles. In this paper, the dynamics of single attosecond pulse generation from a relativistically oscillating plasma mirror is investigated. We use an elementary analytical model as well as particle-in-cell simulations to study few-cycle attosecond pulses. We find that the phase of the field driving the surface oscillations depends on the plasma density and preplasma scale length. This leads us to a counterintuitive conclusion: for the case of normal incidence and a sharp plasma–vacuum boundary, the CEP required for the generation of a single attosecond pulse phase is closer to $\varphi_0 = \pi/2$ (a "sine" pulse), with the exact value depending on the plasma parameters.

I. INTRODUCTION

The advent of femtosecond laser pulses and their nonlinear conversion into phase-locked harmonic frequency combs in the extreme ultraviolet (XUV) spectral region underlies a number of recent developments in the field of attosecond science. In the temporal domain, these frequency combs correspond to attosecond pulses/pulse trains and allow electron dynamics in atoms and condensed matter to be studied on their characteristic temporal and spatial scales.[1,2] The production of harmonic frequency combs is typically achieved through high-order harmonic generation (HHG) in gases[3–6] and is well established. Pulse energies are, however, limited by the modest conversion efficiency. Increasing the pulse energy by converting petawatt class lasers using HHG in gases is impractical owing to the extremely long focal lengths that are needed to achieve the intensities below 10^{15} W cm^{-2} required to optimize HHG in atomic gases.

HHG during the reflection of a relativistically intense laser pulse at plasma surfaces (also referred to as surface HHG)[7,8] is better suited for converting high-peak-power lasers to XUV frequency combs. Substantial progress has been made in the development of the sources in recent years,[9–15] with keV photons[9] and attosecond pulse structure being observed[11] (1 attosecond = 1 as = 10^{-18} s). The higher pulse energies available from surface HHG make it attractive for attosecond pump/attosecond probe experiments, and it is therefore envisaged as a basis of the attosource at the ELI-ALPS[16] project. There are typically three HHG processes under such conditions, so-called coherent wake emission,[11,17] the relativistically oscillating mirror (ROM) mechanism,[18,19] and coherent synchrotron emission (CSE).[20–22] We will concentrate on the ROM and CSE mechanisms,

which are predicted to be better suited to the generation of the shortest pulses.

Clearly, single attosecond pulses are preferable for the measurement of attosecond dynamics. In the case of gas harmonics, a single dominant attosecond pulse is usually produced either with few-cycle laser pulses[3] or with the help of so-called polarization gating.[4,5] The first technique, intensity gating, relies on the shortness of the laser pulse and the nonlinearity of the harmonic generation process. The intensity and maximum photon energy of harmonics depend strongly on the laser field. They will peak in the laser half-cycle with the strongest field. Depending on the carrier-envelope phase (CEP), the laser pulse can have one strong peak (a "cosine" pulse) or two strong peaks of equal strength (a "sine" pulse) in the electric field, leading to a single attosecond pulse or a pair of attosecond pulses. The second technique, polarization gating, relies on the fact that circularly polarized laser pulses do not generate harmonics. By constructing a laser pulse that has circular polarization on the temporal wings of the pulse and linear polarization in the middle, one can effectively gate the harmonic emission process and isolate single attosecond pulses.[23] It is not surprising that similar concepts for generating single attosecond pulses in gases can also be applied in the case of harmonics emitted from plasma surfaces (and nonlinear Compton scattering as well[24,25]). To date, isolated attosecond pulses from surface harmonics have never been measured directly in the laboratory, but experimental[13,15,26–28] and numerical[29–32] results suggest that both intensity and polarization gating will lead to the emission of isolated attosecond pulses.

The influence of the CEP of the ultrashort laser pulses on the HHG process in plasmas has been studied extensively with both laboratory and numerical experiments.[15,33,34] A density-dependent CEP phase shift has not, however, been described. Our work serves as a complementary and, in our opinion, important extension of the above-mentioned papers.

In this paper, we investigate the density and preplasma dependence of the CEP on surface HHG. We show that for the case of normal incidence, the condition for the generation of single attosecond pulses is counterintuitive, requiring careful consideration of the CEP, plasma density, and preplasma scale length. For a dense step-like profile, a "sine" ($\varphi_0 = \pi/2$) rather than the familiar "cosine" ($\varphi_0 = 0$) pulse from HHG in gases is required. The dependence of the CEP phase φ_0 on target density and scale length is investigated both analytically and with 1D and 2D particle-in-cell (PIC) codes (see the left of Fig. 1 for a visualization of the numerical experiment).

Let us note that normal incidence is a crucial aspect of our problem set. With oblique incidence, additional plasma oscillations may occur, as the component of the electric field of the laser, normal to the plasma surface, grows. Oblique counterparts of the 2D PIC simulations presented in this paper show that it is the "cosine" pulse that may produce single attosecond pulses. We omit graphs illustrating this, since they are beyond the scope of this research, but we do refer the reader to relevant material in Ref. 29.

Throughout the paper, relativistic units $m_e = c = e = 1$ are used. The vector potential field amplitude is $a = eA/m_e c$, the time is $t = \omega_L t'$, the momentum is $p = p'/m_e c$, the spatial coordinate is $x = x'/\lambda_L$, and the plasma density is $n = n'/n_c$. Here, c is the speed of light, A is the vector potential describing the laser pulse, ω_L is the laser frequency, $\lambda_L = 2\pi c/\omega_L$ is the laser wavelength, and $n_c = \varepsilon_0 m_e \omega_L^2 e^{-2}$ is the critical density.

II. DENSITY-DEPENDENT PHASE SHIFT

Consider the structure of the fields driving the motion of the electrons at the plasma–vacuum boundary. The transverse electromagnetic fields satisfy the boundary condition equation $a_{\mathrm{inc}} + a_{\mathrm{refl}} = a_{\mathrm{ev}}$, with a_{inc} the incident, a_{refl} the reflected and a_{ev} the evanescent field inside the plasma. At the boundary, electron motion, in addition to being governed by a_{inc}, is also governed by a_{refl}. A phase shift between the incident and reflected fields causes a phase shift of the CEP with respect to the incident laser pulse. This phase shift depends on the detailed form of the evanescent wave that extends into the plasma beyond the critical density surface and consequently on both the peak density and shape of the plasma gradient. This is similar to the phase shift encountered in the reflection of electromagnetic waves from a metallic mirror.

For the analytical model, a preionized overdense ($n_e \gg n_c$) plasma slab occupying the positive half-space ($x \geq 0$) is assumed. Thus, the plasma almost perfectly reflects a linearly polarized relativistic laser pulse incident normally from the negative half-space. The ponderomotive force of the laser pulse causes a fast oscillation of the surface electrons in the longitudinal direction with

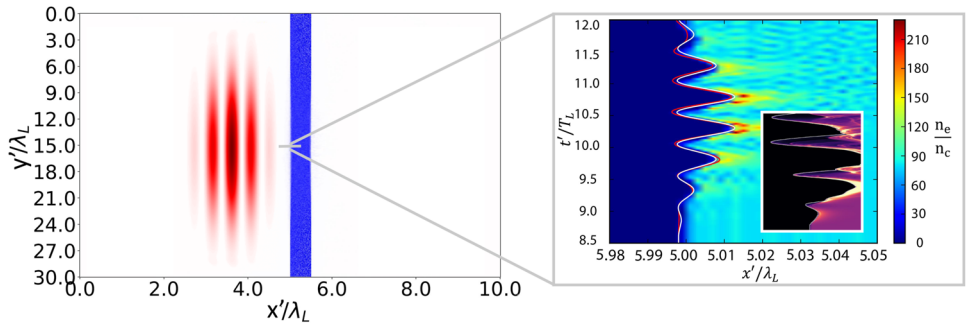

FIG. 1. Left: fixed-time snapshot of 2D PIC experiment before the pulse hits the target. Right: spatio-temporal electron density distribution zoomed on the plasma surface. The white line is the analytical solution and the red line the numerical solution (1D PICWIG) for a single particle. The parameters are $n = 80n_c$, $a_0 = 5$, and a $\sin^2$-enveloped laser pulse with a duration of four optical cycles and linear polarization. The inset on the right shows the evolution of the target density in the relativistic case ($n = 80n_c$, $a_0 = 20$).

near-light-speed velocities. The reflected light is blue-shifted and temporally compressed owing to the relativistic Doppler effect, and thus it contains high-order harmonics.

On the vacuum–plasma boundary, located at $x = 0$, the incident, reflected, and evanescent vector potentials are given by $A_{\mathrm{inc}} = -a_0 \sin(t - x + \varphi_0)$, $A_{\mathrm{refl}} = -a_r \sin(t + x + \varphi_r)$, and $A_{\mathrm{ev}} = -a_t \sin(t + \varphi_t) f(x)$, respectively. Here, $f(x)$ is the function describing the decay of the evanescent wave inside the plasma. Solving the wave equation on the vacuum–plasma boundary, one obtains the boundary conditions

$$a_0 \cos(t + \varphi_0) + a_r \cos(t + \varphi_r) = a_t \cos(t + \varphi_t) f(0) \quad (1)$$

and

$$a_0 \cos(t + \varphi_0) - a_r \cos(t + \varphi_r) = -a_t \sin(t + \varphi_t) f'(0) \quad (2)$$

for the electric and magnetic fields, respectively, at $x = 0$. After some algebraic manipulations, one can see that the resulting electromagnetic fields acting on the electron layer at the plasma surface are phase-shifted relative to the incident fields. This phase shift depends on the value of the evanescent field and its derivative at the boundary, and so the phases of the evanescent and reflected fields are given by

$$\varphi_t = \varphi_0 - \arctan\left[\frac{f'(0)}{f(0)}\right] + 2\pi\nu \quad (3)$$

and

$$\varphi_r = \varphi_0 - 2\arctan\left[\frac{f'(0)}{f(0)}\right] + 2\pi\mu, \quad (4)$$

respectively, where ν and μ are integers. To derive the exact function $f(x)$, one has to solve the wave equation (we assume here $a_0 \ll 1$) $\partial^2 a/\partial t^2 - \partial^2 a/\partial x^2 = -n(x)a(x,t)$ for $x > 0$, i.e., inside the plasma. For a step-like density profile, the resulting phase shift is

$$\varphi_t = \varphi_0 + \arctan\left(\sqrt{\omega_p^2 - \omega_0^2}\right) + 2\pi\nu, \quad (5)$$

where $\omega_p = \sqrt{n_e e^2/(m_e \varepsilon_0)}$ is the plasma frequency of the target, and ω_0 is included to take account of the possibility of using different color mixtures in the incident laser pulse.

If the plasma density increases linearly from 0 to a maximum of n_0 over a distance of L, the phase shift is given by

$$\varphi_t = \varphi_0 + \arctan\left[\frac{-\left(\frac{n_0}{L}\right)^{1/3} \mathrm{Ai}'\left(-\left(\frac{\omega_0}{\omega_L}\right)^2 \left(\frac{n_0}{L}\right)^{-2/3}\right)}{\mathrm{Ai}\left(-\left(\frac{\omega_0}{\omega_L}\right)^2 \left(\frac{n_0}{L}\right)^{-2/3}\right)}\right] + 2\pi\nu, \quad (6)$$

with $\mathrm{Ai}(z)$ being the Airy function and the prime denoting the derivative. As $n_0 \to \infty$, for both a sharp boundary and a linear ramp, the reflected field acquires an additional phase close to π, in accordance with the usual reflection from a perfect mirror.[35]

Note that both the phase φ_t and amplitude a_t of the driving field can be found by solving Eqs. (1) and (2) together with Eq. (3). Knowing the driving vector potential, one can then study the dynamics of the plasma surface using a simple oscillator model.[36] In particular, a comparison of the model calculations with particle trajectories, as well as more details, can be found in Refs. 32 and 36.

An illustration of CEP mechanics is given on the right of Fig. 1, where the plasma dynamics are shown for the case of a normal-incidence interaction with an intense short laser pulse with $a_0 \ll 1$ [where $a_0 = eA/m_e c = I\lambda^2/(1.3 \times 10^{18}\ \mathrm{W\ cm^{-2}\ \mu m^2})$]. The inset shows the relativistic case with $a_0 > 10$: the waveform exhibits distortions. This is due to the nonlinear interaction of the relativistic laser pulse with the plasma, which eventually leads to the emission of attosecond pulses.

The model shows good agreement with PIC simulations for "moderate" values of $a_0 \lesssim \sqrt{n_0/n_c}$, but, for extremely relativistic cases ($a_0 \geq 10$), the elementary model presented above cannot be exact. However, it predicts that the value of the optimal CEP of the laser pulse for the generation of isolated attosecond pulses under normal incidence depends on the plasma parameters (peak density and preplasma length). We shall provide more evidence to support this claim.

In all the 1D simulations that were carried out, we used a $[10\lambda_L \times 16T_L]$ computational grid. We discretized space using 316 points per wavelength and time using 416 points per plasma period. On the spatial axis, an absorbing boundary condition was imposed. The laser pulse was three-cycle and linearly polarized, wrapped in a $\sin^2$ time envelope. The target was located at a distance of $5\lambda_L$ from the laser and had a width of $0.5\lambda_L$. In particular cases, we varied the plasma density, the linear ramp in front of the target, and the laser amplitude and phase. The exact values are given in the corresponding discussions in the text and the figures.

A. Sharp plasma–vacuum boundary

PIC simulations show that in the low-intensity regime ($a_0 \ll 1$), as well as for the subrelativistic case of $a_0 \approx 1$, there is a phase shift between the incident and reflected light, which depends on the density of the target [Figs. 2(a) and 2(b)]. The superposition of incident and reflected fields gives rise to a CEP shift of approximately $\pi/2$ relative to the incident pulse for both densities, with the shift closer to $\pi/2$ for $40n_c$, as predicted by the model. The density-dependent phase shift for typical target densities is sufficient to change the pulse shape from the incident cosine to a sine pulse for the combined incident and reflected fields. Note that negligible surface denting is present in this case.

Increase of the laser intensity further to the relativistic case $1 < a_0 < 10$ drives oscillations in the plasma–vacuum boundary. This is the range of all experiments to date. The nonlinear interaction of the relativistic laser pulse with the plasma leads to the production of high harmonics and eventually attosecond pulses. To obtain the fields driving the electrons, the position of the critical density surface, where the incident laser pulse is reflected, has been calculated, and the incident as well as the reflected field have been obtained at these positions in space and time [see Fig. 2(c)]. The CEP shift of the driving fields relative to the incident field is still clearly visible. This

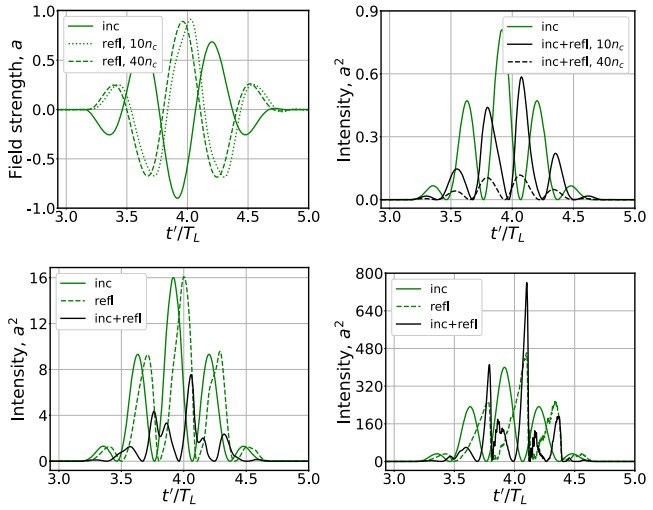

FIG. 2. (a) Field strength and (b) intensity of incident, reflected, and combined fields in the nonrelativistic case for two different densities ($10n_c$ and $40n_c$), with $a_0 = 0.9$. (c) Results of PIC simulations with a laser intensity $a_0 = 4$ and a sharp step in density of $40n_c$. (d) Ultrarelativistic case with $a_0 = 20$ and $80n_c$. The incident and reflected pulse intensities measured at the critical density surface are plotted as solid and dashed green lines, respectively. The combined laser pulse intensity is shown as a solid black line.

behavior remains the same for different intensities and target densities, as long as the magnitude of the driving field, $a_0/\sqrt{1+n}$, stays approximately the same.

For even higher intensities with $a_0 \gg 1$, the driving field at the plasma–vacuum boundary is even more distorted. This coincides with strong oscillations of the plasma surface due to the significant $\mathbf{v} \times \mathbf{B}$ force of the laser pulse at these intensities. The attosecond pulses are generated when electrons are accelerated toward the laser pulse by the electrostatic restoring force (when the momentum p_x toward the laser pulse achieves its maximum and the momentum $p_y = 0$).[37] The reflected field is also highly distorted and enhanced with first harmonics. Although the exact value of the phase shift for a highly distorted pulse is hard to grasp, the basic idea is still visible in Fig. 2(d): the field driving the surface is phase-shifted with respect to the incoming laser pulse.

To check the validity of Eqs. (3)–(6) and to clearly demonstrate the existence of the density-dependent phase shift, we turn to the linear regime, setting $a_0 \ll 1$. The easiest way is to measure the phase of the reflected wave by performing a fast Fourier transform of the data from PIC simulations and comparing it. As we will see later, the phase shift depends on the (relativistically corrected) plasma density through the analytical result in Eq. (4). It is known that in the limiting case of very large values of plasma density (approaching infinity), the resulting phase shift approaches π. For a finite plasma density, the reflected wave phase shift will differ from π depending on the plasma density or, in other words, on the surface impedance.[35]

The dependence of the reflected light phase shift $\Delta\varphi_r = \varphi_r - \varphi_0$ on plasma density is demonstrated in Fig. 3. The green circles represent results obtained by taking the FFT of the reflected field from the one-dimensional PIC simulations for the laser pulse with $a_0 = 0.01$,

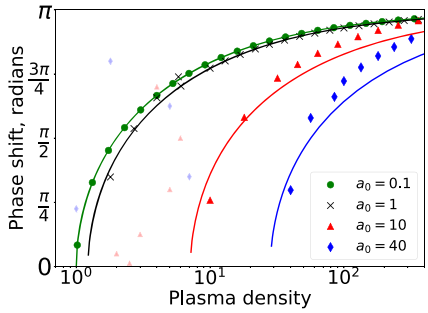

FIG. 3. Dependence of the phase shift of the reflected radiation with respect to the incoming radiation ($\Delta\varphi = \varphi_r - \varphi_0$) on the plasma density for different values of a_0. Curves are given by Eq. (5). For $a \geq 1$, the relativistically corrected plasma density from Eq. (7) is utilized. Smaller and more lightly shaded markers correspond to the cases where the relativistic pulse breaks the too-thin plasma mirror.

and the green solid curve is given by Eq. (5). The analytical and numerical results are in perfect agreement.

Next, PIC simulations were performed for $a_0 = 1$ (the black crosses in Fig. 3). These are very close to the linear case, since the changes in electron mass and density are small. However, to fit the simulation results, we have found that the relativistic correction to the plasma density,

$$n_{0,\mathrm{rel}} = \frac{n_0}{\sqrt{1 + \frac{a_0^2}{2}}} \tag{7}$$

works well (the solid black curve in Fig. 3). To the left of each line on the figure is the area where the target is relativistically transparent and the model breaks down. Such cases are denoted by more lightly shaded and smaller markers to avoid distraction from the main trend. The markers denote the results of PIC simulations, while the solid lines are obtained from Eqs. (5) and (7). The predictions of the model are consistent with the results of PIC simulations, apart from a small offset that grows with increasing laser intensity, from around 0.15 radians at $a_0 = 10$ to around 0.25 radians at $a_0 = 40$. This offset is a result of the increasing longitudinal motion of the plasma surface, which adds both a change in the arrival time of the incident pulse at the surface and a Doppler shift to the reflected pulse.

B. Linear plasma ramp

In the case of a linear preplasma growing from 0 to n_0 over a scale length L, the density-dependent phase shift of the wave driving the oscillations is given by Eq. (6). We can perform a similar analysis to that above to validate this equation.

The dependence of the phase difference of the reflected wave φ_r with respect to the initial CEP φ_0 on the preplasma coefficient n_0/L_λ is presented in Fig. 4. Here, the presence of L_λ means that the coefficient is measured in terms of the laser wavelength. In these and subsequent figures, changing the preplasma coefficient is predominantly done by altering the scale length. However, throughout this paper, there are also corresponding changes in n_0. Such cases will be indicated by stating the value of n_0. Agreement between model and simulations is generally good and clearly demonstrates the dependence of the phase shift on plasma parameters with values close to π for high values of n_0/L_λ. The accuracy is only fair, however, for the

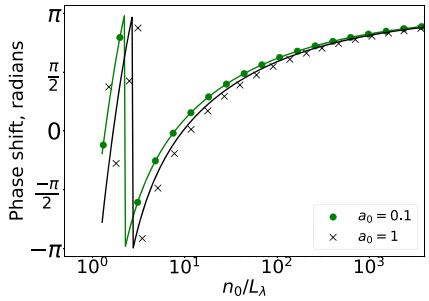

FIG. 4. Dependence of the phase shift of the reflected radiation with respect to the incoming radiation ($\Delta\varphi = \varphi_r - \varphi_0$) on the value of n_0/L_λ for different values of a_0. Results for $a_0 = 0.1$ are shown in green and those for $a_0 = 1$ in black. Curves are given by Eq. (6). For $a_0 = 1$, the relativistically corrected plasma density from Eq. (7) was used. Circles and crosses are the results of 1D PIC simulations.

case of low n_0/L_λ, when the preplasma tends to steepen[39,40] and the analytical model cannot be applied to its full extent. Still, in the area of experimental interest ($n_0/L_\lambda > 1000$), the model fits quite well.

PIC simulations were now run to calculate the reflected wave phase shift with respect to the CEP for different preplasma scale lengths at high laser intensities. The results are presented in Fig. 5. For the areas of experimental interest, the results of the simulations correspond well to the analytical findings.

Let us note that for all cases of high values of n_0 for the sharp boundary and high values of n_0/L for the linear preplasma, the field driving the surface φ_t is approximately $\pi/2$ phase-shifted with respect to the initial laser pulse.

In real interactions, the density ramp is closer to an exponential profile. However, our conclusions obtained for the linear preplasma are also valid for the exponential variant. PIC simulations show similar results for linear and exponential ramps. The scale length at which the density grows from 0 to n_0 is the main parameter that affects the phase shift behavior in both cases.

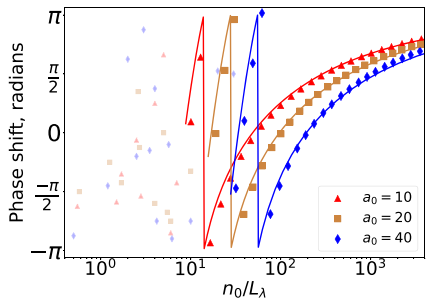

FIG. 5. Dependence of the phase shift of the reflected radiation with respect to the incoming radiation ($\Delta\varphi = \varphi_r - \varphi_0$) on the value of n_0/L_λ for different values of a_0. Results for $a_0 = 10$ are shown by the red curve and triangles, those for $a_0 = 20$ by the brown curve and squares, and those for $a_0 = 40$ by the blue curve and diamonds. The curves are given by Eq. (6), using the relativistically corrected plasma density from Eq. (7), and the markers with the corresponding colors are the results of 1D PIC simulations.

III. CONSEQUENCES FOR ATTOSECOND PULSE GENERATION

In this section, we examine the effects of the density-dependent phase shift described above on the generation of attosecond pulses using few-cycle laser pulses. We examine two generation mechanisms: the relativistically oscillating mirror (ROM)[40] and coherent synchrotron emission (CSE)[22] in transmission. The CEP plays a crucial role in the generation of isolated attosecond pulses. Both the ROM and CSE mechanisms under normal incidence are driven by superposition of the incoming and reflected waves.

For the quasi-linear case of the ROM (where $a_0 \lesssim \sqrt{n}$), the motion of the surface can be described quite well by a simple oscillator model.[36] For stronger drivers, the surface is a highly nonlinear oscillator.[41] However, for a single strong back-swing, which is required for the generation of a single attosecond pulse, the driving electric field has to be a cosine-like ultrashort pulse according to our PIC simulations.

The CSE mechanism relies on the electron nanobunch formed on the front surface of the plasma target. This nanobunch loses its transverse momentum within the plasma skin depth and hence radiates synchrotron emission in the forward direction through the plasma target.[22] In this case, the plasma target itself serves as a low-cut filter. To drive the single nanobunch required for a single attosecond pulse, the driving electric field also has to be a cosine-like short pulse. Owing to the phase shift, the optimal CEP phase for the generation of a single attosecond pulse depends on the plasma conditions and is not unique. Therefore, it has to be chosen correctly.

A. ROM and CSE PIC simulations

Examples of simulations are presented in Fig. 6. In Fig. 6(a), one can see that by way of the ROM mechanism, a "sine" pulse leads to a single reflected attosecond pulse (i.e., the contrast of the main pulse is more than about five times larger than the satellites), whereas a "cosine" pulse leads to a doublet of reflected attosecond pulses. Exactly the same effect can be observed in transmission [Fig. 6(b)].[22] This is because the transmitted XUV pulses are still generated at the surface of the plasma, through the same surface interaction as the reflected XUV pulses, and not in the plasma bulk. Note that no filters were applied to the transmitted pulses—the filtering is done by the target itself. 1D and 2D PIC simulations gave us similar results, and therefore to avoid an excessive number of figures, we only showcase the 2D results in Fig. 6.

Figure 7(a) demonstrates attosecond pulses generated for different CEPs of the laser pulse for a case with $a_0 = 20$, a three-cycle duration of the $\sin^2$ envelope, and a step-like plasma profile with peak density $n_0 = 400$. Reflected light was filtered, cutting down frequencies below the tenth harmonic. The color-coded picture shows the instantaneous attosecond pulse intensity. Four lineouts are demonstrated: one at CEP $\varphi_0 = \pi/2$ (white) corresponding to the initial "sine" pulse, one at CEP $\varphi_0 = 0$ (red) corresponding to the initial "cosine" pulse, one at $\varphi_0 = \pi/4$, and one at $\varphi_0 = 3\pi/4$. Empirically, we find that for a sharp density profile and high values of the density n_0, a "sine" pulse is optimal for the generation of a single attosecond pulse. This is due to the predicted phase shift—the driving field on the surface of the plasma has to be "cosine," which means that initially one has to shoot a "sine" pulse that will be "converted" to a "cosine" pulse. This is different from the case of gas harmonics.

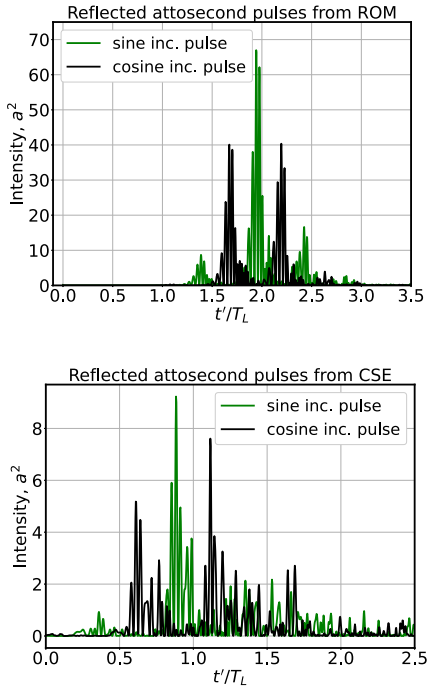

FIG. 6. (a) Attosecond XUV pulses generated by a three-cycle incident pulse with $a_0 = 20$ normally incident on a step-like target with $n_e = 80n_c$. For the ROM, the reflected XUV pulses have been filtered from the 10th to the 30th harmonic. A single XUV pulse is generated only in the case of the sine incident pulse. (b) Generation of attosecond pulse in transmission. Similar to the case of reflection, a sine-shaped incident pulse generates a single XUV pulse in transmission. A cosine-shaped incident pulse generates two distinct transmitted pulses. No filter has been applied to the transmitted pulses.

In the case of a linear density ramp, the optimal CEP value is defined by the best contrast between the main pulse, the prepulse and the trailing pulse to achieve optimal isolation of the single attosecond pulse. For preplasma scale lengths of $\lambda_L/10$, the reflected XUV pulse structure is shown for different CEP values in Fig. 7(b). The target density is $n_e = 400n_c$, and $a_0 = 20$. Incidentally, larger scale length simulations show that cosine laser pulses might again be better. For preplasma coefficients n_0/L_λ as low as 16, this can already be noticed. It is also seen in the plot for $a_0 = 20$ in Fig. 5.

In all simulated cases, $\varphi = \pi/2$ ("sine") is better than $\varphi = 0$ ("cosine"). However, generally speaking, the CEP of the laser pulse has to be chosen carefully according to the plasma parameters.

B. 2D PIC

We also conducted 2D PIC simulations of CEP dependence on the attosecond pulse generation with the PIC code SMILEI.[42] The calculations were performed on a $[10\lambda_L \times 30\lambda_L \times 20T_L]$ computational grid. We discretized with $[400 \times 20]$ points per wavelength in space axes with imposed Silver–Müller boundary conditions and 800 points per plasma period in the time axis. We used a sharp plasma–vacuum boundary setting and an ultra-relativistic scenario: a three-cycle linearly polarized pulse with $a_0 = 20$, normally incident, wrapped in a $\sin^2$ time envelope, and aimed at a step-like target

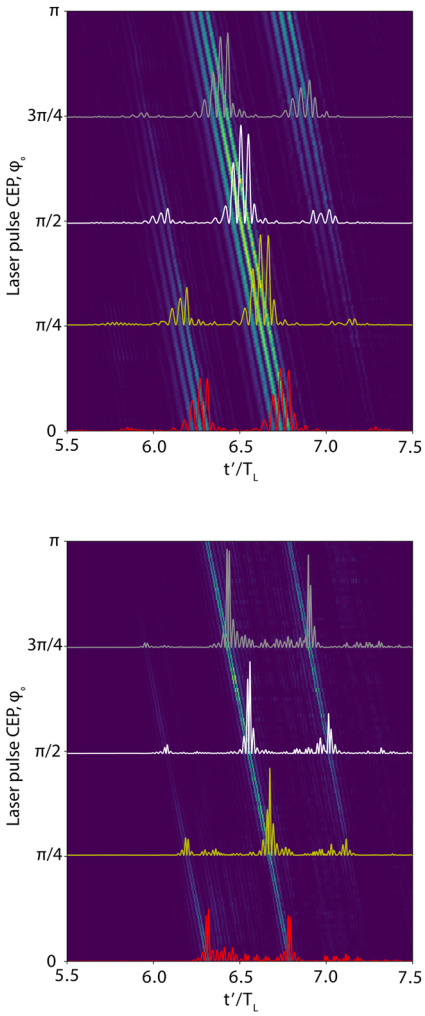

FIG. 7. (a) Dependence of the intensity of the reflected ROM attosecond pulses on time measured in cycles and CEP phase φ_0 of the incoming laser pulse (color-coded image). Colored curves outline the intensity of the attosecond pulses (harmonics with numbers >10) for four different values of φ_0. The laser pulse has $a_0 = 20$, a duration of three cycles, and $n_e = 400n_c$. (b) The same, but in the case when a linear preplasma with length $\lambda_L/10$ is added to the target.

with $n_e = 80n_c$. The target was located at a distance $5\lambda_L$ from the laser and had a width of $0.5\lambda_L$. The laser was focused right at the middle of the target $(x'/\lambda_L = 5, y'/\lambda_L = 15)$ and had a waist = $10\lambda_L$.

Figure 8 shows the reflections of incident "cosine" and "sine" pulses from the ROM and pulses in transmission as a result of the CSE mechanism. The simulation confirms that the "sine" laser pulse generates a single-peak intensity attosecond pulse, whereas the "cosine" laser pulse generates a train of two attosecond pulses for both cases. One can see the reflected pulses [Fig. 6(a)] and the pulses in transmission [Fig. 6(b)] detected on the laser axis (at $y'/\lambda_L = 15$). In both cases, one sees distinct single-peak and two-peak pulses generated from "sine" and "cosine" pulses, respectively.

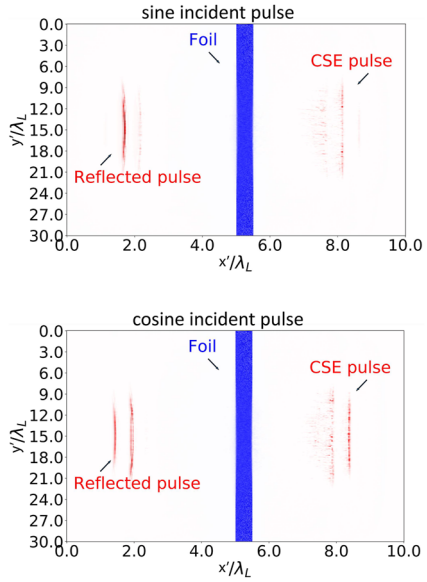

FIG. 8. Intensity of reflected pulses and pulses in transmission in 2D, showing that the result is independent of the simulation code and the dimensionality. (a) corresponds to the reflected pulse and CSE pulse of the incident "sine" pulse, and (b) corresponds to the reflected pulse and CSE pulse of the incident "cosine" pulse. Incident pulses had an amplitude of $a_0 = 20$, and the target density in all cases was $n_e = 80n_c$.

IV. CONCLUSION

We have shown analytically and with the help of PIC simulations that in the case of a high-density step profile, one can easily find the ideal CEP ("sine" pulses are better than "cosine" in normal incidence). However, when the density is reduced, or the plasma scale length increased, it becomes more complicated, since the phase of the reflected pulse varies accordingly. Then, the ideal CEP is no longer trivial. When compared with harmonic generation from gaseous media, the behavior is counterintuitive, in that a so-called sine-shaped incident laser pulse with two intensity maxima of equal strength produces a single attosecond pulse from a step-like overdense plasma target.

The reason for this behavior across all intensity regimes is a phase shift between the incident laser pulse and the electromagnetic field driving the motion of the surface electrons, with higher-order effects coming into play at the highest intensities. This phase shift depends on the density of the plasma target and the length of the preplasma. Thus, the conditions for generating the brightest attosecond XUV pulse, namely, a high transverse momentum of the electrons and a high velocity antiparallel to the incident pulse, are only met once during the interaction, despite the incident pulse exhibiting two peaks of equal intensity.

For a plasma target with preplasma, a parameter scan using 1D PIC simulations has been used to determine the optimal CEP for a given preplasma length, showing complex interplay between the plasma oscillations and the driving laser. Our results demonstrate that both the CEP and the plasma density distribution have to be carefully taken into account in experiments on generation of single attosecond pulses from surface HHG.

ACKNOWLEDGMENTS

Some of the simulations were performed using the Skoltech CDISE supercomputer Zhores.[43] This work was supported by the Russian Science Foundation (Grant No. 22-22-01031).[44]

AUTHOR DECLARATIONS

Conflict of Interest

The authors have no conflicts to disclose.

Author Contributions

Rishat Zagidullin: Software (equal); Validation (equal). **Stefan Tietze**: Visualization (equal); Writing – original draft (equal). **M. Zepf**: Conceptualization (equal); Formal analysis (equal); Methodology (equal). **Jingwei Wang**: Conceptualization (equal); Formal analysis (equal); Methodology (equal); Writing – review & editing (equal). **Sergey G. Rykovanov**: Conceptualization (equal); Formal analysis (equal); Methodology (equal); Writing – review & editing (equal).

DATA AVAILABILITY

Data sharing is not applicable to this article as no new data were created or analyzed in this study. Simulation and visualization scripts are available from the corresponding author upon reasonable request.

REFERENCES

[1] F. Krausz and M. Ivanov, "Attosecond physics," Rev. Mod. Phys. **81**, 163–234 (2009).
[2] G. Sansone, L. Poletto, and M. Nisoli, "High-energy attosecond light sources," Nat. Photonics **5**, 655–663 (2011).
[3] A. Baltuška, T. Udem, M. Uiberacker, M. Hentschel, E. Goulielmakis, C. Gohle, R. Holzwarth, V. Yakovlev, A. Scrinzi, T. Hänsch, and F. Krausz, "Attosecond control of electronic processes by intense light fields," Nature **421**, 611–615 (2003).
[4] G. Sansone, E. Benedetti, F. Calegari, C. Vozzi, L. Avaldi, R. Flammini, L. Poletto, P. Villoresi, C. Altucci, R. Velotta, S. Stagira, S. De Silvestri, and M. Nisoli, "Isolated single-cycle attosecond pulses," Science **314**, 443 (2006).
[5] P. Tzallas, E. Skantzakis, C. Kalpouzos, E. Benis, G. Tsakiris, and D. Charalambidis, "Generation of intense continuum extreme-ultraviolet radiation by many-cycle laser fields," Nat. Phys. **3**, 846–850 (2007).
[6] M. Lewenstein, P. Balcou, M. Ivanov, A. L'Huillier, and P. Corkum, "Theory of high-harmonic generation by low-frequency laser fields," Phys. Rev. A **49**, 2117–2132 (1994).
[7] R. Lichters, J. Meyer-ter Vehn, and A. Pukhov, "Short-pulse laser harmonics from oscillating plasma surfaces driven at relativistic intensity," Phys. Plasmas **3**, 3425–3437 (1996).
[8] P. Norreys, M. Zepf, S. Moustaizis, A. Fews, J. Zhang, P. Lee, M. Bakarezos, C. Danson, A. Dyson, P. Gibbon, P. Loukakos, D. Neely, F. Walsh, J. Wark, and A. Dangor, "Efficient extreme UV harmonics generated from picosecond laser pulse interactions with solid targets," Phys. Rev. Lett. **76**, 1832–1835 (1996).
[9] B. Dromey, M. Zepf, A. Gopal, K. Lancaster, M. Wei, K. Krushelnick, M. Tatarakis, N. Vakakis, S. Moustaizis, R. Kodama, M. Tampo, C. Stoeckl, R. Clarke,

H. Habara, D. Neely, S. Karsch, and P. Norreys, "High harmonic generation in the relativistic limit," Nat. Phys. **2**, 456–459 (2006).
[10]B. Dromey, D. Adams, R. Hörlein, Y. Nomura, S. Rykovanov, D. Carroll, P. Foster, S. Kar, K. Markey, P. McKenna, D. Neely, M. Geissler, G. Tsakiris, and M. Zepf, "Diffraction-limited performance and focusing of high harmonics from relativistic plasmas," Nat. Phys. **5**, 146–152 (2009).
[11]Y. Nomura, R. Horlein, P. Tzallas, B. Dromey, S. Rykovanov, Z. Major, J. Osterhoff, S. Karsch, L. Veisz, M. Zepf, D. Charalambidis, F. Krausz, and G. Tsakiris, "Attosecond phase locking of harmonics emitted from laser-produced plasmas," Nat. Phys. **5**, 124–128 (2009).
[12]F. Quéré, C. Thaury, J.-P. Geindre, G. Bonnaud, P. Monot, and P. Martin, "Phase properties of laser high-order harmonics generated on plasma mirrors," Phys. Rev. Lett. **100**, 095004 (2008).
[13]P. Heissler, R. Hörlein, M. Stafe, J. Mikhailova, Y. Nomura, D. Herrmann, R. Tautz, S. Rykovanov, I. Földes, K. Varjú, F. Tavella, A. Marcinkevicius, F. Krausz, L. Veisz, and G. Tsakiris, "Toward single attosecond pulses using harmonic emission from solid-density plasmas," Appl. Phys. B **101**, 511–521 (2010).
[14]C. Rödel, D. an der Brügge, J. Bierbach, M. Yeung, T. Hahn, B. Dromey, S. Herzer, S. Fuchs, A. Pour, E. Eckner, M. Behmke, M. Cerchez, O. Jäckel, D. Hemmers, T. Toncian, M. Kaluza, A. Belyanin, G. Pretzler, O. Willi, A. Pukhov, M. Zepf, and G. Paulus, "Harmonic generation from relativistic plasma surfaces in ultrasteep plasma density gradients," Phys. Rev. Lett. **109**, 125002 (2012).
[15]P. Heissler, R. Hörlein, J. Mikhailova, L. Waldecker, P. Tzallas, A. Buck, K. Schmid, C. Sears, F. Krausz, L. Veisz, M. Zepf, and G. Tsakiris, "Few-cycle driven relativistically oscillating plasma mirrors: A source of intense isolated attosecond pulses," Phys. Rev. Lett. **108**, 235003 (2012).
[16]S. Mondal, M. Shirozhan, N. Ahmed, M. Bocoum, F. Boehle, A. Vernier, S. Haessler, R. Lopez-Martens, F. Sylla, C. Sire, F. Quéré, K. Nelissen, K. Varjú, D. Charalambidis, and S. Kahaly, "Surface plasma attosource beamlines at ELI-ALPS," J. Opt. Soc. Am. B **35**, A93 (2018).
[17]F. Quéré, C. Thaury, P. Monot, S. Dobosz, P. Martin, J.-P. Geindre, and P. Audebert, "Coherent wake emission of high-order harmonics from overdense plasmas," Phys. Rev. Lett. **96**, 125004 (2006).
[18]U. Teubner and P. Gibbon, "High-order harmonics from laser-irradiated plasma surfaces," Rev. Mod. Phys. **81**, 445–479 (2009).
[19]C. Thaury and F. Quéré, "High-order harmonic and attosecond pulse generation on plasma mirrors: Basic mechanisms," J. Phys. B: At., Mol. Opt. Phys. **43**, 213001 (2010).
[20]D. an der Brügge and A. Pukhov, "Enhanced relativistic harmonics by electron nanobunching," Phys. Plasmas **17**, 033110 (2010).
[21]B. Dromey, S. Cousens, S. Rykovanov, M. Yeung, D. Jung, D. Gautier, T. Dzelzainis, D. Kiefer, S. Palaniyppan, R. Shah, J. Schreiber, J. Fernandez, C. Lewis, M. Zepf, and B. Hegelich, "Coherent synchrotron emission in transmission from ultrathin relativistic laser plasmas," New J. Phys. **15**, 015025 (2013).
[22]B. Dromey, S. Rykovanov, M. Yeung, R. Hörlein, D. Jung, D. Gautier, T. Dzelzainis, D. Kiefer, S. Palaniyppan, R. Shah, J. Schreiber, H. Ruhl, J. Fernandez, C. Lewis, M. Zepf, and B. Hegelich, "Coherent synchrotron emission from electron nanobunches formed in relativistic laser–plasma interactions," Nat. Phys. **8**, 804–808 (2012).
[23]V. Platonenko and V. Strelkov, "Single attosecond soft-x-ray pulse generated with a limited laser beam," J. Opt. Soc. Am. B **16**, 435 (1999).
[24]M. Valialshchikov, V. Kharin, and S. Rykovanov, "Narrow bandwidth gamma comb from nonlinear Compton scattering using the polarization gating technique," Phys. Rev. Lett. **126**, 194801 (2021).
[25]M. Valialshchikov, V. Kharin, and S. Rykovanov, "Polarisation gating technique in nonlinear Compton scattering: Effect of radiation friction and electron beam nonideality," Quantum Electron. **51**, 812 (2021).
[26]A. Borot, A. Malvache, X. Chen, A. Jullien, J.-P. Geindre, P. Audebert, G. Mourou, F. Quéré, and R. Lopez-Martens, "Attosecond control of collective electron motion in plasmas," Nat. Phys. **8**, 416–421 (2012).
[27]M. Yeung, B. Dromey, S. Cousens, T. Dzelzainis, D. Kiefer, J. Schreiber, J. Bin, W. Ma, C. Kreuzer, J. Meyer-ter Vehn, M. Streeter, P. Foster, S. Rykovanov, and M. Zepf, "Dependence of laser-driven coherent synchrotron emission efficiency on pulse ellipticity and implications for polarization gating," Phys. Rev. Lett. **112**, 123902 (2014).
[28]M. Yeung, J. Bierbach, E. Eckner, S. Rykovanov, S. Kuschel, A. Sävert, M. Förster, C. Rödel, G. Paulus, S. Cousens, M. Coughlan, B. Dromey, and M. Zepf, "Noncollinear polarization gating of attosecond pulse trains in the relativistic regime," Phys. Rev. Lett. **115**, 193903 (2015).
[29]G. Tsakiris, K. Eidmann, J. Meyer-ter Vehn, and F. Krausz, "Route to intense single attosecond pulses," New J. Phys. **8**, 19 (2006).
[30]G. Ma, W. Dallari, A. Borot, F. Krausz, W. Yu, G. Tsakiris, and L. Veisz, "Intense isolated attosecond pulse generation from relativistic laser plasmas using few-cycle laser pulses," Phys. Plasmas **22**, 033105 (2015).
[31]L. Liu, C. Xia, J. Liu, W. Wang, Y. Cai, C. Wang, R. Li, and Z. Xu, "Control of single attosecond pulse generation from the reflection of a synthesized relativistic laser pulse on a solid surface," Phys. Plasmas **15**, 103107 (2008).
[32]S. Rykovanov, M. Geissler, J. Meyer-ter Vehn, and G. Tsakiris, "Intense single attosecond pulses from surface harmonics using the polarization gating technique," New J. Phys. **10**, 025025 (2008).
[33]D. Kormin, A. Borot, G. Ma, W. Dallari, B. Bergues, M. Aladi, I. Földes, and L. Veisz, "Spectral interferometry with waveform-dependent relativistic high-order harmonics from plasma surfaces," Nat. Commun. **9**, 4992 (2018).
[34]O. Jahn, V. Leshchenko, P. Tzallas, A. Kessel, M. Krüger, A. Münzer, S. Trushin, G. Tsakiris, S. Kahaly, D. Kormin, L. Veisz, V. Pervak, F. Krausz, Z. Major, and S. Karsch, "Towards intense isolated attosecond pulses from relativistic surface high harmonics," Optica **6**, 280–287 (2019).
[35]B. I. Bleaney and B. Bleaney, *Electricity and Magnetism*, 3rd ed. (Oxford University Press, London, 1976).
[36]S. Rykovanov, H. Ruhl, J. Meyer-ter Vehn, R. Hörlein, B. Dromey, M. Zepf, and G. Tsakiris, "Plasma surface dynamics and smoothing in the relativistic few-cycle regime," New J. Phys. **13**, 023008 (2011).
[37]J. Jackson, *Classical Electrodynamics*, 3rd ed. (Wiley, New York, 1998).
[38]M. Geissler, S. Rykovanov, J. Schreiber, J. Meyer-ter Vehn, and G. Tsakiris, "3D simulations of surface harmonic generation with few-cycle laser pulses," New J. Phys. **9**, 218 (2007).
[39]B. Dromey, S. Rykovanov, D. Adams, R. Hörlein, Y. Nomura, D. Carroll, P. Foster, S. Kar, K. Markey, P. McKenna, D. Neely, M. Geissler, G. Tsakiris, and M. Zepf, "Tunable enhancement of high harmonic emission from laser solid interactions," Phys. Rev. Lett. **102**, 225002 (2009).
[40]S. Bulanov, N. Naumova, and F. Pegoraro, "Interaction of an ultrashort, relativistically strong laser pulse with an overdense plasma," Phys. Plasmas **1**, 745 (1994).
[41]A. Debayle, J. Sanz, L. Gremillet, and K. Mima, "Toward a self-consistent model of the interaction between an ultra-intense, normally incident laser pulse with an overdense plasma," Phys. Plasmas **20**, 053107 (2013).
[42]J. Derouillat, A. Beck, F. Pérez, T. Vinci, M. Chiaramello, A. Grassi, M. Flé, G. Bouchard, I. Plotnikov, N. Aunai, J. Dargent, C. Riconda, and M. Grech, "SMILEI: A collaborative, open-source, multi-purpose particle-in-cell code for plasma simulation," Comput. Phys. Commun. **222**, 351–373 (2018).
[43]I. Zacharov, R. Arslanov, M. Gunin, D. Stefonishin, A. Bykov, S. Pavlov, O. Panarin, A. Maliutin, S. Rykovanov, and M. Fedorov, "'Zhores'—Petaflops supercomputer for data-driven modeling, machine learning and artificial intelligence installed in Skolkovo Institute of Science and Technology," Open Eng. **9**, 512–520 (2019).
[44]https://rscf.ru/project/22-22-01031/, 2022.